

Supporting Information

Highly clean and efficient iron phosphates modified by Ru nanocrystals for water oxidation

*Min Jiang, Xiaoyue Hu, Pengfei Tan *, and Jun Pan **

State Key Laboratory for Powder Metallurgy, Central South University Lushan South Street 932, Changsha 410083, China.

*Corresponding authors

Email addresses: jun.pan@csu.edu.cn; tpf0203@csu.edu.cn

Characterizations:

Scanning electron microscopy (SEM) and Transmission electron microscopy (TEM) characterizations were performed on a Nova Nano SEM 230 and TecnaiG2 20ST electron microscopies to obtain the morphology of samples. In order to having a good knowledge of compositions of samples, X-ray diffraction analysis (XRD) data were obtained on a Rigaku-TTRIII diffractometer with Cu-K α radiation, and X-ray photoelectron spectrometer (XPS) measurements were conducted on a K-Alpha 1063 photoelectron spectrometer. Raman and Fourier Transform Infrared Spectroscopy (FTIR) data were individually derived from LabRAM HR800 and Nicolet iS50 equipment. Weight percent of metal ion was achieved from inductively coupled plasma-optical emission spectroscopy (ICP-OES, Aglient 5110). The Thermogravimetry (TG) curve and real-time Fourier Transform Infrared (FTIR) Spectroscopy were characterized through Gas chromatograph-mass spectrometer (GCMS, GCMS-Q2010U1TRA).

Electrochemical measurements:

All the OER catalytic measurements were carried out with a CHI660E workststion with 80 mL of 1.0 M KOH electrolyte in a tandard three-electrode system, which used a modified Ni foam as the working electrode, a Pt foil as the counter electrode as well as an Ag/AgCl electrode as the reference electrode. The elaborate synthesis of working electrode were described as bellow: Firstly, 2 mg of typical sample was dissolved and sonicated in mixed solvents of 96 μ L of ethanol and 4 μ L of 5 wt% Nafion, then a piece of Ni foam ($1 \times 1.5 \text{ cm}^2$) was dispersed by mixed ink and occupied with $1 \times 1 \text{ cm}^2$ area.

After drying at 40 °C for 6h, the modified electrode could be used for electrochemical characterizations. First of all, cyclic voltammetry (CV) tests were performed for 50 cycles at 50 mV s⁻¹ from 0 to 0.1 V vs. Ag/AgCl to stimulate the catalytic activities. Then, the linear sweep voltammetry (LSV) with 90% *iR* compensation was performed at 5 mV s⁻¹ from 0 to 0.8 V vs. Ag/AgCl. Subsequently, the electrochemical impedance spectroscopy (EIS) tests were conducted from 100 kHz to 0.1 Hz, and the CV tests proceed varying with at 20, 40, 60, 80, and 300 mV s⁻¹. Based on the Ag/AgCl electrode, the overpotential (η) was computed using the following equation:

$$E_{\text{RHE}} = E_{\text{Ag/AgCl}} + E^{\circ}_{\text{Ag/AgCl}} + 0.059 \text{ pH}$$

$$\eta_{\text{OER}} = E_{\text{RHE}} - 1.23 \text{ V.}$$

Calculation of turn over frequency (TOF) values

As illustrated in the literature, the TOF value during OER can be calculated from the formula: $\text{TOF} = j \times N_A / (4 \times n \times F)$ (j = Current density, N_A = Avogadro number, F = Faraday constant). n represents the number of surface active sites, which can be achieved from the equation: $n = Q / (1 \times 1.602 \times 10^{-19})$. Charge (Q) can be derived from the formula: $Q = \text{peak area}/v$. v is a specific scan rate, in this work we select 300 mV/s as the specific scan rate; then the peak area was obtained from the reductive negative scan peak area of cyclic voltammograms at 300 mV s⁻¹.

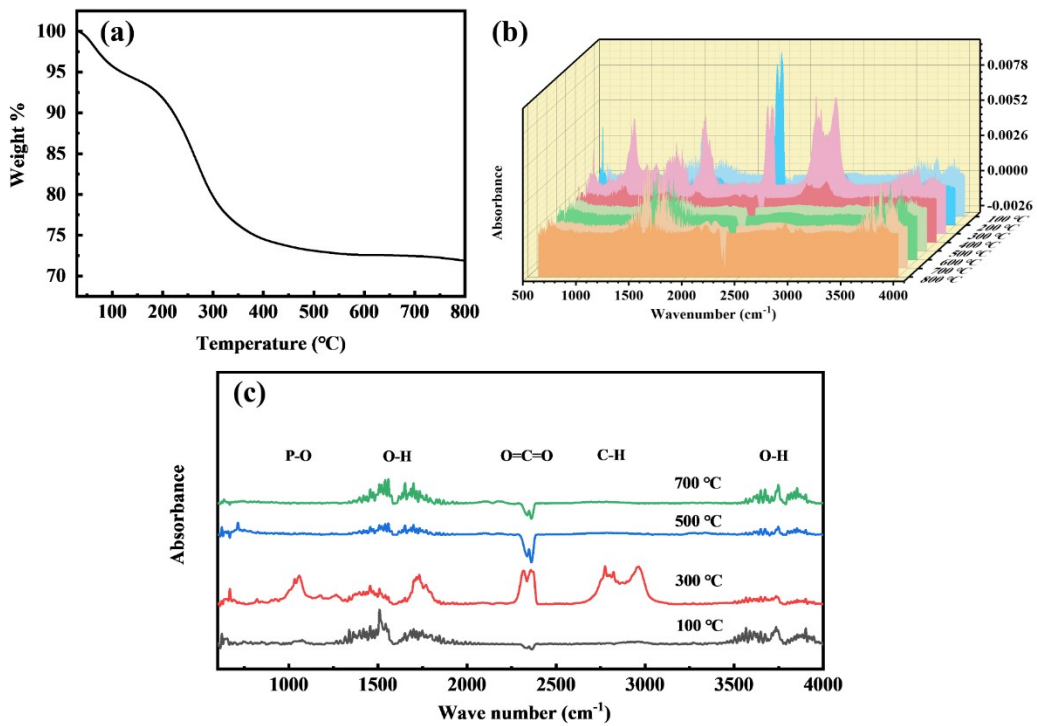


Fig. S1 The thermogravimetry (TG) curve of RFP-2 precursor (a), the three-dimensional Fourier Transform Infrared (FTIR) Spectroscopy of volatile products during pyrolysis of RFP-2 precursor (b), and FTIR spectra at particular temperatures (c).

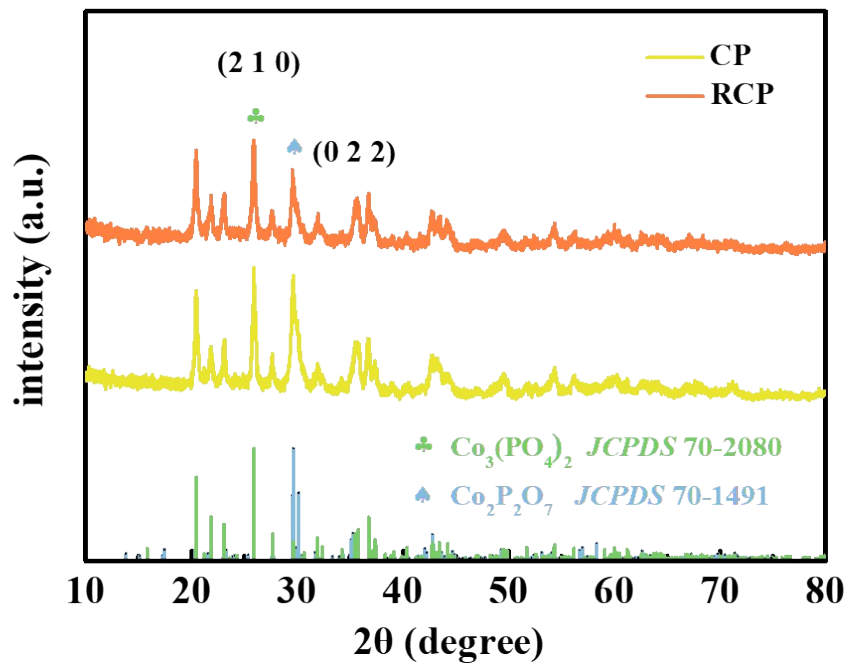


Fig. S2 XRD patterns of CP and RCP.

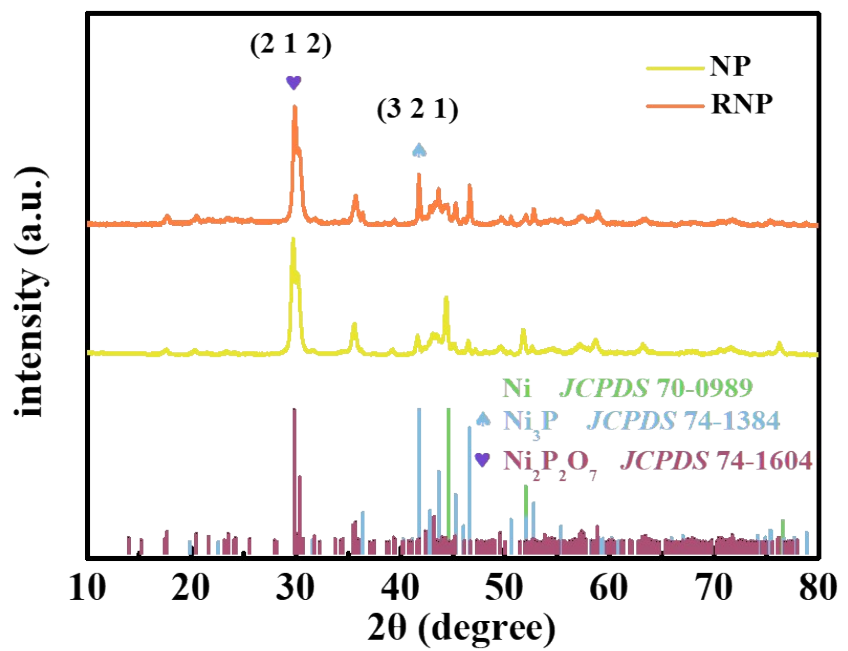


Fig. S3 XRD patterns of NP and RNP.

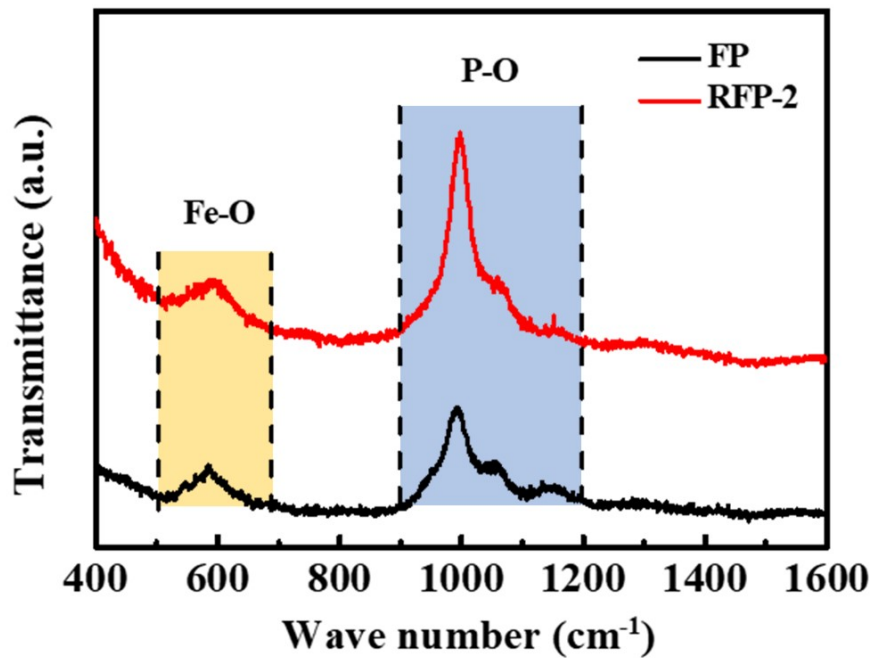


Fig. S4 Raman spectra of samples.

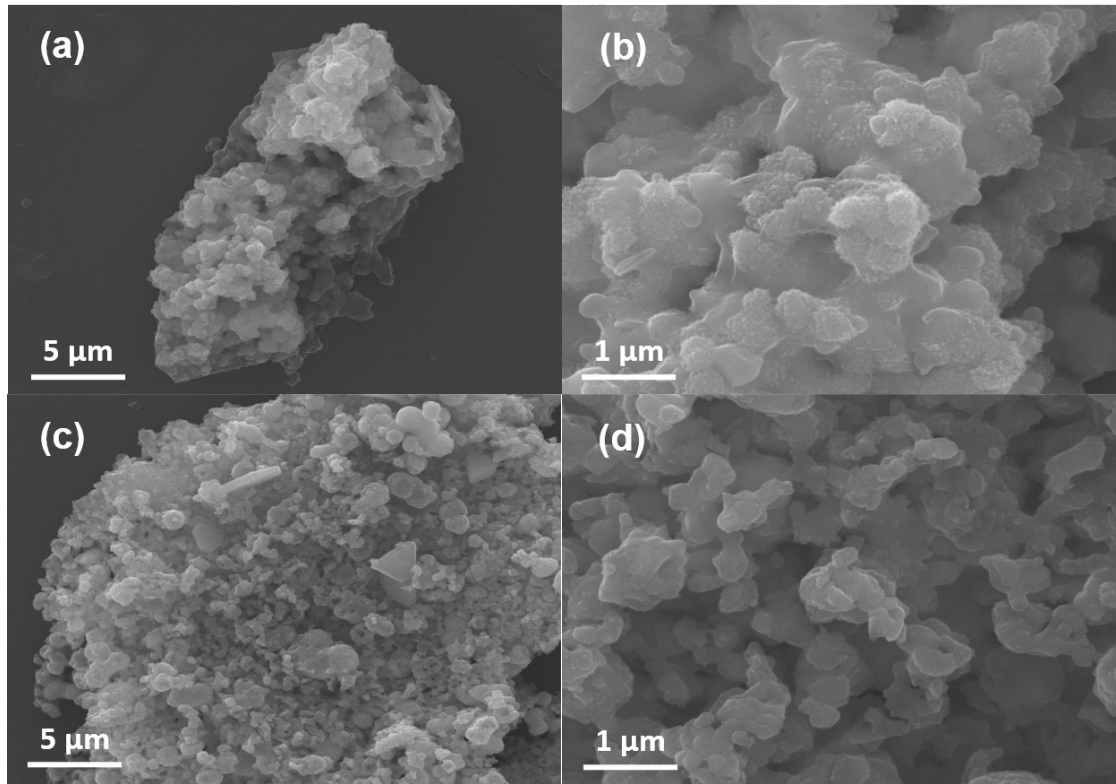


Fig. S5 The SEM images of FP (a and b) and RFP-2 (c and d) at the scale bar of 10 μm

and 2 μm .

Table S1 The corresponding parameters derived from XPS results

	Name	Start eV	BE Peak eV	BE End BE eV	Height CPS	FWHM eV	Atomic %
FP	Fe2p	737.54	710.50	703	13039.36	4.23	12.48
	P2p	139	133.30	125	5236.72	1.91	8.8
	O1s	540	530.81	526	36482.66	2.1	43.26
	C1s	296	284.30	281	14823.06	1.46	35.32
RFP-2	Fe2p	737.88	710.45	703	20706.81	4.35	16.81
	P2p	139	133.45	125	9396.88	1.79	12.21
	O1s	540	531.03	526	59621.76	1.69	52.43
	C1s	296	284.3	281	8956.6	1.55	18.13
	Ru3p	492.34	461.46	450	542.35	2.81	0.42
RFP-2 after CA tests	Fe2p	742.03	710.67	698.13	483.89	7.94	
	P2p	143.68	133.14	123.78	107.35	2.45	
	O1s	536.83	530.87	527.93	7602.2	1.81	
	Ru3p	492.98	486.61	478.48	110.65	3.02	

Table S2 The summary of the main benchmark systems on electrochemical OER catalysts based on first row transition metals.

Catalysts	Electrolytes	Overpotential (η_i , mV)	Tafel slope (mV dec ⁻¹)	Ref.
TMB				
Ni _x B	1.0 M KOH	380 (i=10 mA cm ⁻²)	89	1 ^[1]
FeB ₂	1.0 M KOH	300 (i=10 mA cm ⁻²)	52	2 ^[2]
Ni ₃ B/Ni foam	1.0 M KOH	300 (i=10 mA cm ⁻²)	43	3 ^[3]
FeCoNiBO _x	1.0 M KOH	290 (i=10 mA cm ⁻²)	47	4 ^[4]
TMO				
Co ₃ O ₄ /Ni foam	1.0 M KOH	340 (i=10 mA cm ⁻²)	108	5 ^[5]
NiCo ₂ O ₄	1.0 M KOH	320 (i=10 mA cm ⁻²)	30	6 ^[6]
Co ₃ O ₄ @CoO	0.5 M KOH	430 (i=10 mA cm ⁻²)	89	7 ^[7]
NiFe/NiCo ₂ O ₄	1.0 M KOH	320 (i=10 mA cm ⁻²)	51	8 ^[8]
Ni _x Co _{3-x} O ₄	1.0 M NaOH	380 (i=10 mA cm ⁻²)	65	9 ^[9]
TM-LDH				
NiCo-LDH	1.0 M KOH	370 (i=10 mA cm ⁻²)	40	10 ^[10]
NiFe-LDH/CNT	1.0 M KOH	250 (i=5 mA cm ⁻²)	31	11 ^[11]
FeNi-rGO LDH	1.0 M KOH	200 (i=10 mA cm ⁻²)	39	12 ^[12]
NiFe-LDH NSs	1.0 M KOH	300 (i=10 mA cm ⁻²)	40	13 ^[13]
TMS				
Ni ₃ S ₂	1.0 M KOH	330 (i=10 mA cm ⁻²)	52	14 ^[14]

Fe-CoMoS	1.0 M KOH	280 (i=10 mA cm ⁻²)	58	15 ^[15]
NSs/rGO	1.0 M KOH	200 (i=10 mA cm ⁻²)	40	16 ^[16]
FeSx/CoSx	1.0 M KOH	300 (i=10 mA cm ⁻²)	49	17 ^[17]
TMS_e				
CoSe ₂ NSs	0.1 M KOH	320 (i=10 mA cm ⁻²)	44	18 ^[18]
NixFe _{1-x} Se ₂	1.0 M KOH	200 (i=10 mA cm ⁻²)	28	19 ^[19]
CeO ₂ /CoSe ₂	0.1 M KOH	290 (i=10 mA cm ⁻²)	44	20 ^[20]
NiSe ₂ /FeSe ₂	1.0 M KOH	240 (i=10 mA cm ⁻²)	35	21 ^[21]
TMP(i)				
Co ₂ P	1.0 M KOH	370 (i=10 mA cm ⁻²)	128	22 ^[22]
CoMnP	1.0 M KOH	330 (i=10 mA cm ⁻²)	61	22 ^[22]
Ni ₂ P	1.0 M KOH	290 (i=10 mA cm ⁻²)	59	23 ^[23]
FeP-rGO	1.0 M KOH	260 (i=10 mA cm ⁻²)	50	24 ^[24]
Co-Fe-P-O	1.0 M KOH	270 (i=10 mA cm ⁻²)	30	25 ^[25]
CoFePi-H3	1.0 M KOH	250(i=10 mA cm ⁻²)	35	26 ^[26]
TMA				
FeCoNi	0.5 M KOH	400 (i=10 mA cm ⁻²)	72	27 ^[27]
N-rGO-CoFe	0.1 M KOH	220 (i=10 mA cm ⁻²)	94	28 ^[28]
NiCo NCAs	1.0 M KOH	330 (i=10 mA cm ⁻²)	69	29 ^[29]
CoNi@NCNTs	1.0 M KOH	370 (i=10 mA cm ⁻²)	74	30 ^[30]

Note: TMB, TMO, TM-LDH, TMS, TMSe, TMP(i), TMA are corresponding transition metal base borides, oxides, layer double hydroxides, sulfides, selenides, phosphides/phosphates, and alloys, respectively.

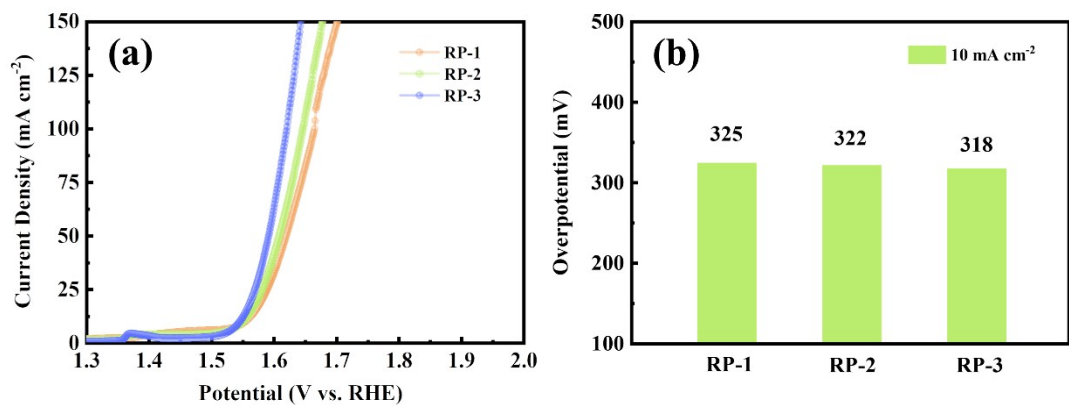


Fig. S6 LSV curves (a) and the corresponding Overpotential bar graph of RP-1, RP-2, and RP-3 at $j = 10 \text{ mA cm}^{-2}$ (b).

Table S3 Summary of overpotentials of transition metal phosphide analogues for OER.

Sample	$\eta_j = 10 \text{ mA cm}^{-2}$	Electrolyte	Ref.
FeP	260	1.0 M KOH	31 ^[31]
CoP ₃ NAs/CFP	334	1.0 M KOH	32 ^[32]
Ni ₂ P/rGO	260	1.0 M KOH	33 ^[33]
Co ₂ P/Co-Foil	319	1.0 M KOH	34 ^[34]
CNTs@NiCoP/C	297	1.0 M KOH	35 ^[35]
Mn-Co-P YS	330	1.0 M KOH	36 ^[36]
(Co _{0.54} Fe _{0.46}) ₂ P	370	0.1 M KOH	37 ^[37]
CoMn/C-HHPNC	262	1.0 M KOH	38 ^[38]
FeP@GPC	278	1.0 M KOH	39 ^[39]
NiCuP	300	1.0 M KOH	40 ^[40]

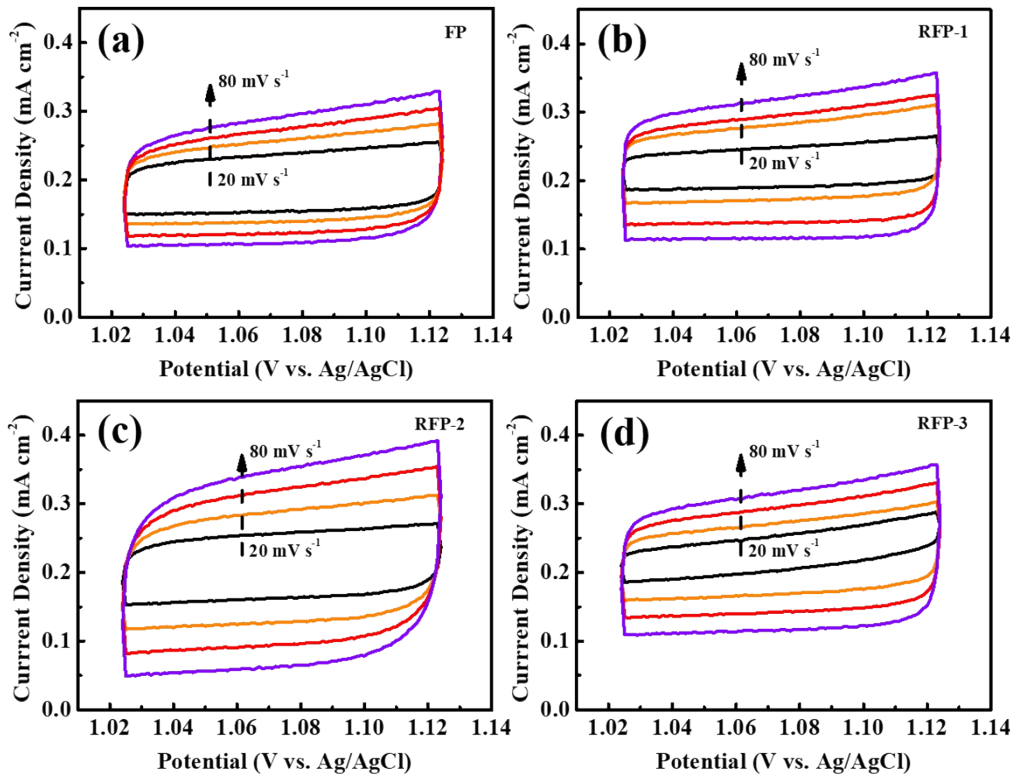


Fig. S7 CV curves of FP, RFP-1, RFP-2, and RFP-3 at 20, 40, 60, and 80 mV s^{-1} .

Table S4 Parameters obtained from the fitted plots measured at 0.394 V using the relevant equivalent circuit.

Samples	R_s (Ω)	R_{ct} (Ω)	CPE-T (F)	CPE-P (F)
FP	2.104	0.996	0.002	0.868
RFP-1	1.975	0.881	0.003	0.838
RFP-2	1.824	0.671	0.007	0.848
RFP-3	1.896	1.391	0.003	0.796

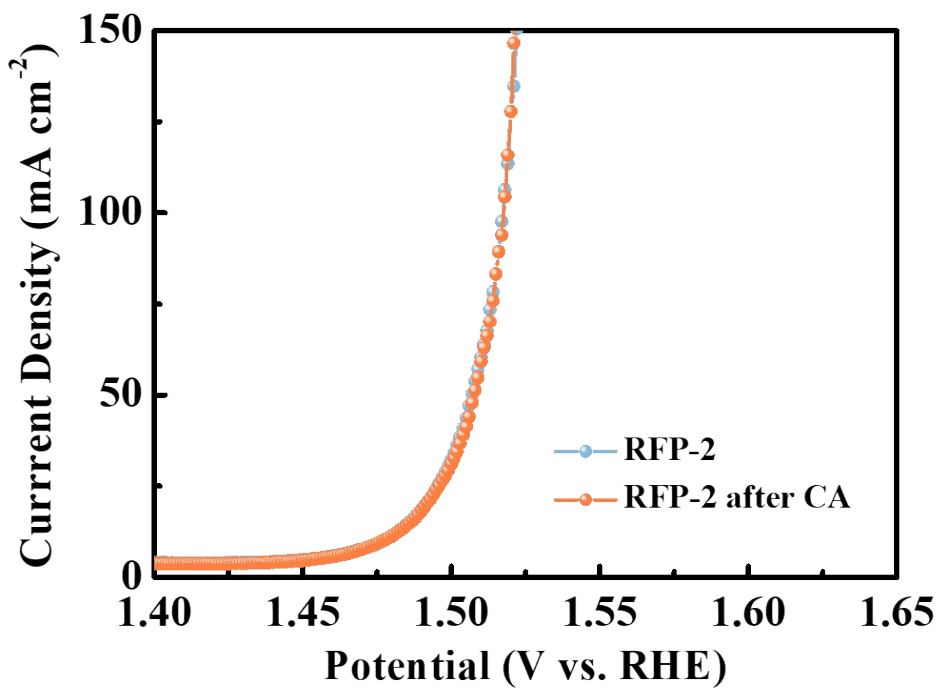


Fig. S8 The LSV comparison of RFP-2 and RFP-2 after CA tests.

References

1. J. Masa, I. Sinev, H. Mistry, E. Ventosa, M. de la Mata, J. Arbiol, M. Muhler, B. Roldan Cuenya and W. Schuhmann, *Adv Energy Mater*, 2017, **7**, 1700381.
2. H. Li, P. Wen, Q. Li, C. C. Dun, J. H. Xing, C. Lu, S. Adhikari, L. Jiang, D. L. Carroll and S. M. Geyer, *Adv Energy Mater*, 2017, **7**, 1700513.
3. J. H. Li, H. Chen, Y. P. Liu, R. Q. Gao and X. X. Zou, *J Mater Chem A*, 2019, **7**, 5288-5294.
4. H. Mao, X. Guo, Y. L. Fu, H. R. Yang, Y. Zhang, R. Zhang and X. M. Song, *J Mater Chem A*, 2020, **8**, 1821-1828.
5. Y. Q. Zhang, B. Ouyang, J. Xu, G. C. Jia, S. Chen, R. S. Rawat and H. J. Fan, *Angew Chem Int Edit*, 2016, **55**, 8670-8674.
6. J. Bao, X. D. Zhang, B. Fan, J. J. Zhang, M. Zhou, W. L. Yang, X. Hu, H. Wang, B. C. Pan and Y. Xie, *Angew Chem Int Edit*, 2015, **54**, 7399-7404.
7. C. W. Tung, Y. Y. Hsu, Y. P. Shen, Y. X. Zheng, T. S. Chan, H. S. Sheu, Y. C. Cheng and H. M. Chen, *Nat Commun*, 2015, **6**.
8. C. L. Xiao, Y. B. Li, X. Y. Lu and C. Zhao, *Adv Funct Mater*, 2016, **26**, 3515-3523.
9. L. J. Enman, M. S. Burke, A. S. Batchellor and S. W. Boettcher, *Acs Catal*, 2016, **6**, 2416-2423.
10. H. F. Liang, F. Meng, M. Caban-Acevedo, L. S. Li, A. Forticaux, L. C. Xiu, Z. C. Wang and S. Jin, *Nano Lett*, 2015, **15**, 1421-1427.
11. M. Gong, Y. G. Li, H. L. Wang, Y. Y. Liang, J. Z. Wu, J. G. Zhou, J. Wang, T.

- Regier, F. Wei and H. J. Dai, *J Am Chem Soc*, 2013, **135**, 8452-8455.
12. X. Long, J. K. Li, S. Xiao, K. Y. Yan, Z. L. Wang, H. N. Chen and S. H. Yang, *Angew Chem Int Edit*, 2014, **53**, 7584-7588.
13. F. Song and X. L. Hu, *Nat Commun*, 2014, **5**.
14. X. R. Zheng, X. P. Han, Y. Q. Zhang, J. H. Wang, C. Zhong, Y. D. Deng and W. B. Hu, *Nanoscale*, 2019, **11**, 5646-5654.
15. Y. N. Guo, X. Zhou, J. Tang, S. Tanaka, Y. V. Kaneti, J. Na, B. Jiang, Y. Yamauchi, Y. S. Bando and Y. Sugahara, *Nano Energy*, 2020, **75**.
16. J. Jiang, S. Lu, W. K. Wang, G. X. Huang, B. C. Huang, F. Zhang, Y. J. Zhang and H. Q. Yu, *Nano Energy*, 2018, **43**, 300-309.
17. M. Wang, C. L. Dong, Y. C. Huang and S. H. Shen, *Acs Catal*, 2020, **10**, 1855-1864.
18. Y. W. Liu, H. Cheng, M. J. Lyu, S. J. Fan, Q. H. Liu, W. S. Zhang, Y. D. Zhi, C. M. Wang, C. Xiao, S. Q. Wei, B. J. Ye and Y. Xie, *J Am Chem Soc*, 2014, **136**, 15670-15675.
19. X. Xu, F. Song and X. L. Hu, *Nat Commun*, 2016, **7**.
20. Y. R. Zheng, M. R. Gao, Q. Gao, H. H. Li, J. Xu, Z. Y. Wu and S. H. Yu, *Small*, 2015, **11**, 182-188.
21. Y. S. Du, G. Z. Cheng and W. Luo, *Catal Sci Technol*, 2017, **7**, 4604-4608.
22. D. Li, H. Baydoun, C. N. Verani and S. L. Brock, *J Am Chem Soc*, 2016, **138**, 4006-4009.
23. L. A. Stern, L. G. Feng, F. Song and X. L. Hu, *Energ Environ Sci*, 2015, **8**, 2347-

24. J. Masud, S. Umapathi, N. Ashokaan and M. Nath, *J Mater Chem A*, 2016, **4**, 9750-9754.
25. D. Q. Yin, Z. Y. Jin, M. M. Liu, T. T. Gao, H. Y. Yuan and D. Xiao, *Electrochim Acta*, 2018, **260**, 420-429.
26. S. A. Khalate, S. A. Kadam, Y. R. Ma, S. B. Kulkarni, V. G. Parale and U. M. Patil, *J Colloid Interf Sci*, 2022, **613**, 720-732.
27. S. Saha and A. K. Ganguli, *Chemistryselect*, 2017, **2**, 1630-1636.
28. A. Samanta and C. R. Raj, *J Phys Chem C*, 2018, **122**, 15843-15852.
29. B. Zhang, X. M. Zhang, Y. Wei, L. Xia, C. R. Pi, H. Song, Y. Zheng, B. Gao, J. J. Fu and P. K. Chu, *J Alloy Compd*, 2019, **797**, 1216-1223.
30. J. J. Huo, L. Lu, Z. Y. Shen, H. Gao and H. Liu, *Surf Innov*, 2021, **9**, 37-48.
31. J. Masud, S. Umapathi, N. Ashokaan, M. Nath, Iron phosphide nanoparticles as an efficient electrocatalyst for the OER in alkaline solution, *J Mater Chem A* **2016**, *4*, 9750-9754.
32. T. L. Wu, M. Y. Pi, D. K. Zhang, S. J. Chen, 3D structured porous CoP₃ nanoneedle arrays as an efficient bifunctional electrocatalyst for the evolution reaction of hydrogen and oxygen, *J Mater Chem A* **2016**, *4*, 14539-14544.
33. L. T. Yan, H. M. Jiang, Y. L. Xing, Y. Wang, D. D. Liu, X. Gu, P. C. Dai, L. J. Li, X. B. Zhao, Nickel metal-organic framework implanted on graphene and incubated to be ultrasmall nickel phosphide nanocrystals acts as a highly efficient water splitting electrocatalyst, *J Mater Chem A* **2018**, *6*, 1682-1691.

34. C. Z. Yuan, S. L. Zhong, Y. F. Jiang, Z. K. Yang, Z. W. Zhao, S. J. Zhao, N. Jiang, A. W. Xu, Direct growth of cobalt-rich cobalt phosphide catalysts on cobalt foil: an efficient and self-supported bifunctional electrode for overall water splitting in alkaline media, *J Mater Chem A* **2017**, *5*, 10561-10566.
35. Y. J. Zhao, G. L. Fan, L. Yang, Y. J. Lin, F. Li, Assembling Ni-Co phosphides/carbon hollow nanocages and nanosheets with carbon nanotubes into a hierarchical necklace-like nanohybrid for electrocatalytic oxygen evolution reaction, *Nanoscale* **2018**, *10*, 13555-13564.
36. Y. V. Kaneti, Y. N. Guo, N. L. W. Septiani, M. Iqbal, X. C. Jiang, T. Takei, B. Yuliarto, Z. A. Alothman, D. Golberg, Y. Yamauchi, Self-templated fabrication of hierarchical hollow manganese-cobalt phosphide yolk-shell spheres for enhanced oxygen evolution reaction, *Chemical Engineering Journal* **2021**, *405*, 126580.
37. A. Mendoza-Garcia, D. Su, S. H. Sun, Sea urchin-like cobalt-iron phosphide as an active catalyst for oxygen evolution reaction, *Nanoscale* **2016**, *8*, 3244-3247.
38. G. L. Li, X. B. Zhang, H. Zhang, Ultrathin 2D nanosheet based 3D hierarchical hollow polyhedral CoM/C (M = Ni, Cu, Mn) phosphide nanocages as superior electrocatalysts toward oxygen evolution reaction, *Chemical Engineering Journal* **2020**, *398*, 125467.
39. Y. D. Yao, N. Mahmood, L. Pan, G. Q. Shen, R. R. Zhang, R. J. Gao, F. E. Aleem, X. Y. Yuan, X. W. Zhang, J. J. Zou, Iron phosphide encapsulated in P-doped graphitic carbon as efficient and stable electrocatalyst for hydrogen and

oxygen evolution reactions, *Nanoscale* **2018**, *10*, 21327-21334.

40. L. Wei, K. Goh, O. Birer, H. E. Karahan, J. Chang, S. L. Zhai, X. C. Chen, Y. Chen, A hierarchically porous nickel-copper phosphide nano-foam for efficient electrochemical splitting of water, *Nanoscale* **2017**, *9*, 4401-4408.